J. Fluid Mech. (1996), vol. 316, pp. 285–306

Measurement of the lift force on a particle fixed to the wall in the viscous sublayer of a fully developed turbulent boundary layer

By A. M. MOLLINGER[1,2]† AND F. T. M. NIEUWSTADT[1]

[1]Department of Mechanical Engineering, Delft University of Technology, Lab for Aero- and Hydrodynamics, Rotterdamseweg 145, 2628 AL, Delft, The Netherlands

[2]Department of Chemical Engineering, Delft University of Technology, Lab for Particle Technology, Julianalaan 136, 2628 BL, Delft, The Netherlands

(Received 2 January 1995 and in revised form 6 February 1996)

We have investigated the lift force on a small isolated particle which is attached to a flat smooth surface and embedded within the viscous sublayer of the turbulent boundary layer over this surface. We have developed a novel experimental technique with which it is possible to measure both the mean and fluctuating lift force by gluing the particle on top of a silicium cantilever. The deflection of this cantilever is measured with a focused laser beam. The sensitivity of the focus detection system allows us to measure a lift force with an average value around 10^{-8}N and with a standard deviation of approximately 5% of the mean. This means that our device is at least a factor of 100 more sensitive than previous devices and at the same time able to measure the lift forces on smaller particles. Data for the mean lift force (F_L^+) as a function of the particle radius (a^+), where both parameters have been non-dimensionalized with the kinematic viscosity ν and the friction velocity u_*, are obtained in the range $0.3 < a^+ < 2$. The data support the relationship: $F_L^+ = (56.9 \pm 1.1)\,(a^+)^{1.87\pm0.04}$. Also results on the fluctuating lift force have been obtained. We find that the ratio of the r.m.s. to the mean lift force is approximately 2.8.

1. Introduction

The force on a small particle attached to a flat surface and embedded in a shear flow is not only interesting from a pure fluid mechanics point of view but it also has many applications. Examples are entrainment and resuspension of particles occurring in erosion due to e.g. sand or dust storms and in the motion of sediments or sand at the bottom of rivers and lakes. Human activity may also cause particle entrainment, e.g. dust from coal stockpiles. The forces on particles in the neighbourhood of a surface are also important for the opposite case of deposition on a wall for example in the chemical industry where one is interested in the behaviour of catalyst particles near a wall.

In this study we restrict ourselves to one of the forces that acts on a single particle attached to a smooth and flat surface, namely the lift force. This force, in combination with the other forces that act on the particle, such as gravity, adhesion and drag, plays a role in its resuspension. However, a lift force large enough to be able to separate the

† Present address: Shell Research b.v., Volmerlaan 8, 2288 GD, Rijswijk, The Netherlands.

particle from the surface is only one of the mechanisms responsible for resuspension. It may also be caused by particle interactions, such as collisions followed by rolling motions. For an extensive overview of these processes leading to resuspension we refer to Bagnold (1961) and Philips (1980).

We aim to measure in a turbulent boundary layer the lift force on a particle, so small that it is totally embedded in the so-called viscous sublayer. This is the region of the turbulent boundary layer nearest to the wall. As the name suggests, the flow in this layer is dominated by viscous forces. However, the flow is also influenced by the turbulence above the viscous sublayer and therefore highly non-stationary. This means that apart from a mean lift force on the particle due to the mean shear, we can also expect a strongly fluctuations force. This fact together with the rather small magnitude of the force makes this a non-trivial experiment.

Let us first review the previous attempts to measure the lift force on a particle that have been reported in the literature. One of the first was Jeffreys (1929) who tried to measure the force on a cylinder. From his simple laboratory experiments, the accuracy of which he questioned himself, no significant lift force could be deduced. Bagnold (1974) measured the forces on moving and rotating bodies in a boundary layer flow in a water channel. The bodies were a cylinder, 8 cm long, and a sphere. Both were 1.6 cm in diameter and so they spanned several regimes of the boundary layer. These experiments established the existence of a lift force acting on the particles and that this force points away from the wall. Eichhorn & Small (1964) measured the lift and drag force on small spherical particles near a wall in an axisymmetric Poiseuille flow. The diameters of the spheres ranged from 1.5 to 3.2 mm. They attempted to obtain a direct correlation between the lift force and other parameters, such as the particle Reynolds number, the flow velocity and the position of the sphere in the tube. A power-law relationship was suggested but, unfortunately, the data were not sufficiently extensive to reliably define this relationship.

The first lift force sensor for a single particle fixed to the wall was designed by Hille, Megens & Tessmer (1982). The sensor was later modified and further experiments were done by Radecke & Schulz-Dubois (1988). This lift sensor used very large particles, about 1 cm in diameter, in a water channel. Another lift force sensor was developed by Hall (1988) for smaller particles, 1 to 5 mm in diameter, in a wind tunnel. Rosenthal & Sleath (1986) measured the lift force on a particle in an oscillatory flow in a water channel in order to study sediment transport. The apparatus is almost the same as the one used by Radecke & Schulz-Dubois. They observed the lift force as a function of the oscillating frequency and of the height of the free surface above the wall.

All these lift force sensors were based on the same basic design, i.e. a small particle attached to a rod or wire that is guided through a small hole in the wall. The lift force was measured with strain gauges connected to the rod or wire. Here, we shall consider the set-up of Hall in somewhat more detail as background for our own experiments. His apparatus was installed in a wind tunnel and used to measure the lift force on particles with a diameter of 1–5 mm. The particles, which were in the lower part of a turbulent boundary layer, were attached to a thin tungsten wire that passed through a narrow hole in the surface and was centered by means of three bronze sheet springs to avoid contact between the wall and the wire. The distance between the particle and the plate could be varied by manipulating the mounting system under the surface. The force sensing element was a commercially available force transducer and the geometric arrangement of the transducer was chosen such that movement of the transducer load button was predominantly along one direction. The system could be tilted in order to minimize the influence of the drag force on the measured lift

force. Based on his experiments Hall presented the following relationship between the mean lift force (F_L) and the particle radius (a):

$$\frac{F_L}{\rho v^2} = (20.90 \pm 1.57)\left(\frac{au_*}{v}\right)^{2.31\pm0.02}, \tag{1.1}$$

where ρ is the density and v is the kinematic viscosity of the fluid; u_* is the friction velocity to be defined in §4. In all experiments of Hall, the particle penetrated the viscous sublayer and protruded into the buffer layer or even the logarithmic layer. It is then no longer subjected to a mean velocity with constant shear only, as is the case for particles completely embedded in the viscous sublayer and this may have influence on the lift force.

The lift force on a small particle in a shear flow has been also the subject of many theoretical studies. All these theories apply primarily to small particle Reynolds numbers, i.e. $au_p/v \leqslant 0.01$, where u_p is a characteristic velocity scale, because in this case the so-called Stokes approximation can be applied. However to calculate the lift force, the Stokes equations are not sufficient due to their property of time reversibility. This means that the inertia terms to a first-order correction (the Oseen approximation) must be included although it should be noted that in the presence of a wall the Oseen approximation does not include all the leading-order effects of inertia.

Saffman (1965) derived an expression for the lift force on a sphere in a linear unbounded shear flow:

$$F_L = \frac{6.46v\rho a^2 V\kappa^{0.5}}{v^{0.5}}, \tag{1.2}$$

where V is the difference between the velocity of the particle centre and of the undisturbed flow at the position of the centre and κ denotes the velocity gradient. Saffman states that if one includes higher-order approximations an additional term is found, so that the total lift force becomes

$$F_L = \frac{6.46v\rho a^2 V\kappa^{0.5}}{v^{0.5}} - \frac{11}{8}\rho V\kappa a^3. \tag{1.3}$$

Saffman emphasizes that other additional terms of the same order as this one come from the outer expansion. However these additional terms are not calculated and therefore only relation (1.2) should be used in the calculations. Leighton & Acrivos (1985) have studied the lift force on a particle fixed to a wall in a linear shear flow. They show that the lift force is positive so that the particle experiences a force away from the wall. This lift force is given by

$$F_L = 9.22\kappa\rho v a^2\left(\frac{\kappa a^2}{v}\right). \tag{1.4}$$

For further theoretical results we refer to McLaughlin (1989, 1991, 1993) and Cherukat & McLaughlin (1994). In the latter publication a rather complete treatment is given of the force on a small particle in a shear flow in the neighbourhood of a surface. The two theoretical expressions (1.2) and (1.4) are found to be limiting cases.

Given the results discussed above, some points should be noted. First the experimental set-up of Hille *et al.* (1982), Rosenthal & Sleath (1986), Radecke & Schulz-Dubois (1988) and Hall (1988), which are all based on a similar design, presents a number of problems. For instance, bending of the support needle of the particle may result in contact with the wall of the hole and consequently in friction which in turn may influence the lift force measurement. Also the limited sensitivity and stability of the piezo-electric elements or the strain gauges may cause problems.

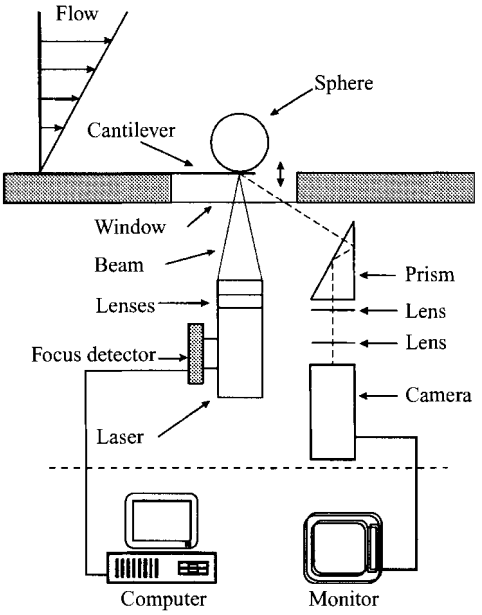

FIGURE 1. Schematic of the new experimental set-up.

Furthermore, the particles used were mostly so large that they extended beyond the viscous sublayer and are thus not representative for a particle in a linear shear flow. Finally, all the previous experimental studies have only considered the mean force, while we know that the lift force on the particle is highly non-stationary. With respect to the theoretical investigations, we may again mention that they are only valid for very small particle Reynolds numbers. In many practical situations the Reynolds number is $O(1)$ and it is far from clear how the theoretical results should be extrapolated to this range of Reynolds numbers.

Considering these points, we feel that accurate information on the lift force on a small sphere immersed in the viscous sublayer of a turbulent boundary layer and at particle Reynolds numbers of $O(1)$ is still lacking, especially with respect to the fluctuations of this force. The latter is especially important when one needs information on the instantaneous lift force, e.g. to determine resuspension of a particle. Therefore, measurement of this fluctuating lift force is the goal that we pursue in this research. For this we have designed and built a new measuring device with which we have carried out experiments.

In the following section we will give a brief description of the experimental set-up. In §3 we discuss our measurement procedure. The measurement results and their analysis are presented in §4. Finally in §5 comparison with theory is discussed.

2. Experimental set-up

To measure the fluctuating lift force on a small particle we have developed a new measuring device capable measurements with a mean value of around 10^{-8}N and with sensitivity of approximately 10^{-10}N. The time resolution is 50 kHz. The experimental set-up is schematically shown in figure 1. A detailed description of this set-up is given by Mollinger, Nieuwstadt & Bessem (1995), so that we will restrict ourselves here to a short discussion.

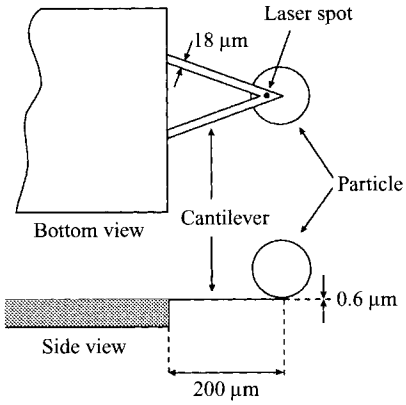

FIGURE 2. Silicium cantilever with particle and laser spot.

A spherical particle is glued onto a flexible silicium springboard (cantilever). This cantilever is placed flush with the surface of the flat plate. Owing to the lift force exerted on the particle the cantilever bends slightly upward. This deflection is measured by means of a diode laser with additional optics (focus detector). A camera is installed to monitor the correct position of the diode-laser spot on the cantilever. Most of the measurements have been carried out with a hollow glass particle with a diameter, $d_p = 120 \pm 1$ μm. For some observations we have also used a solid plastic (sepharose) particle (density 1500 kg m^{-3}) with a diameter of 218 μm.

The flat plate, which we will call the measuring plate, is mounted together with the lift-measuring device in the measuring section of a closed circuit wind tunnel. The tunnel velocity can be varied between 0 and 12 m s^{-1}. The contraction ratio of the settling chamber to the measuring section is 1.8. The measuring section has a cross-section of 60 cm times 60 cm with a total length of 6 m. The measuring plate is made of aluminium and has a length of 5 m. It is mounted at a distance of approximately 20 cm above the bottom wall of the wind tunnel. On the plate a turbulent boundary layer develops generated by a trip wires 60 cm from the leading edge. The upper and lower walls of the wind tunnel are adjusted to compensate for the boundary layer growth so that a condition of zero pressure gradient is maintained over the measuring plate. In the measuring plate the lift force sensor is installed at 3.0 m from the leading edge, where the thickness of the boundary layer is approximately 30 mm.

The cantilever on which the particle is glued is shown in more detail in figure 2. The cantilever is made of silicium and is coated with gold on the back side for increased optical reflection. The force constant, defined as the ratio between the force exerted at the point of the cantilever and the resulting deflection of the cantilever, has been specified by the manufacturer (Park Scientific Instruments) as 0.032 ± 2 N m^{-1}. This value has been checked by modelling the measuring device with a solid glass particle as a simple linear spring and by calculating the resonance frequency. The result was found to agree with the spectral peak of time series observed for this particle (see §4). Given the force constant the lift force on the particle can now be calculated from the deflection.

The laser system (wavelength=780 nm) used to measure the deflection of the cantilever is a distance-measuring system based on the principle of a focus detection technique. The whole system can be considered as a light pen. Such a system is able to measure displacements which are much smaller than the wavelength of the laser

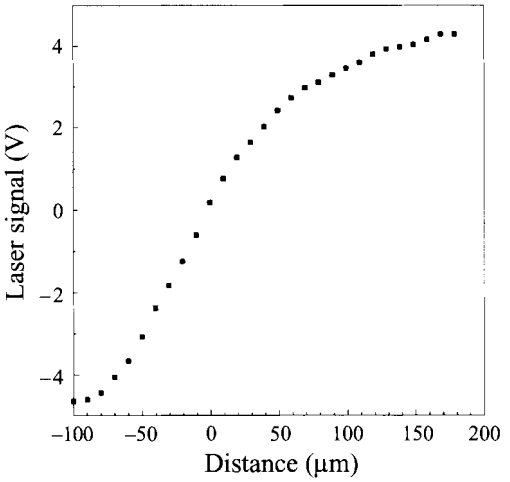

FIGURE 3. Distance–voltage curve (0 mV is in focus, 'negative' distance – laser too close to the cantilever, 'positive' distance – laser too far from the cantilever).

light used, e.g. an optimized standard system can measure displacements of 1 nm and better. For further details regarding this technique we refer to Bouwhuis *et al.* (1985). The system that we employ and which is originally part of a Philips CD player (Mark1 CD module/CDM1), has been slightly modified by adding some optical components (see figure 1). The focus-error signal of the light pen is shown as a function of distance in figure 3, where zero volt means perfect focus and thus zero displacement. For the measurement of the cantilever displacement the steep portion of the curve (see figure 3) around 0 mV is used. In this region there is a linear relationship between the displacement and the electrical signal. A typical displacement of the cantilever of 1.00 ± 0.01 μm results in a voltage change of the signal of 66.7 ± 0.1 mV. The calibration was achieved by traversing the laser beam towards and away from the cantilever over a known distance and recording the voltage change produced.

For visual inspection and positioning of the laser spot a ccd camera is used. The image of the cantilever is directly projected on a ccd chip connected to a television monitor. The whole measuring system, i.e. distance measuring system, electronics, traversing units, lenses and ccd camera has been built together in a single unit which is attached to the underside of the measuring plate, and which is enclosed in a cylindrical container with a streamline fairing on the outside to avoid disturbance to the wind tunnel flow.

To check for possible bias in the lift force measurements and also to investigate any influence of the construction of the device on the measurements, we have performed the following tests.

First, experiments have been carried out without a sphere attached to the cantilever. This allows us to investigate the effect of the vibrations of the wind tunnel and the surroundings (most of the experiments were carried out at night to reduce such vibrations) and also the influence of turbulent pressure fluctuations. Some of the measured statistical quantities of these experiments are given in table 1(*a*). These show a mean lift force close to zero with a small standard deviation mainly due to fluctuations at 50 Hz related to the power source. The magnitude of this spectral peak is only 0.1% of the value measured at this frequency with the particle installed. For a more extensive data set we refer to Mollinger (1995).

u_0 (m s^{-1})	$F^+_{L,modal}$	$\sigma_{F^+_L}$	Skewness	Kurtosis
(*a*)				
0.0	5.60×10^{-2}	4.58	-2.60×10^{-2}	2.97
3.0	-3.73×10^{-2}	4.68	-5.14×10^{-3}	2.99
6.0	3.60×10^{-1}	4.91	-2.77×10^{-2}	3.16
9.0	-4.14×10^{-1}	5.05	1.32×10^{-3}	3.06
12.0	3.54×10^{-1}	5.42	1.64×10^{-2}	3.26
(*b*)				
0.0	-3.71×10^{-1}	4.63	2.90×10^{-2}	3.04
3.0	-4.71×10^{-1}	4.75	6.89×10^{-4}	3.01
6.0	2.39×10^{-1}	4.69	5.99×10^{-3}	2.99

TABLE 1. Statistical quantities of the dimensionless lift force (*a*) with no particle attached to the cantilever, and (*b*) Statistical quantities of the dimensionless lift force with a spherical plastic particle (d_p = 218 μm) attached to the cantilever under a cover (Mean lift force = 0).

Second, a large spherical plastic particle was attached to the cantilever. A cover was placed over the particle in order to investigate the effect of the vibrations of the system under tunnel operating conditions. This cover could only be used at speeds below 9 m s^{-1}. The measured statistical quantities for the cantilever with cover are given in table 1(*b*). The results show the standard deviation σ_F to be quite similar to the case with no particle given in table 1, for the same reason. The contribution due to noise from vibration was estimated to be less than 0.1%.

Moreover, it can be concluded from the values for the skewness and the kurtosis also given in table 1 that the measured distributions are highly symmetrical and that they are close to Gaussian.

Based on the results of these tests, we conclude that the effect of vibrations and pressure fluctuations on the measured statistics of the lift force is negligible. Furthermore, we have found that if no particle is attached to the cantilever, no significant lift force is measured. This gives us confidence that we are indeed measuring the lift force on the particle due to the flow and that our measurements are not disturbed by additional unknown effects.

The air velocity is measured with a constant-temperature hot-wire anemometer (single wire) with a sensitive element of 0.5 mm length and a diameter of 2.5 μm. The hot-wire anemometer was calibrated before and after each run against a Pitot tube attached to a Betz manometer within the same wind tunnel. The hot wire is used to measure the profile of the horizontal velocity component by traversing it normal to the plate. It appeared that there was no measurable effect of the cantilever (with or without a particle) on the velocity profile. Horizontal traverses showed that the flow was uniform (within 0.5%) in the spanwise direction.

3. Measurement procedure

The lift force measurements are all carried out using the following experimental procedure.

(1) Calibration of the hot wire at a position 12 cm above the measuring plate (i.e. in the middle of the wind tunnel far above the boundary layer). The calibration of the hot-wire anemometer with the Pitot tube is corrected for pressure and temperature effects.

(2) Visual inspection of the cantilever by means of the ccd camera to check the position of the laser spot of the distance measuring system on the cantilever.

(3) Adjustment and calibration of the displacement measurement device, after which a sensitivity test is performed to check if the device was still operating on the steep part of the curve shown in figure 3.

(4) Measurement of the lift force (with a free-stream velocity between 0.8 m s^{-1} and 12 m s^{-1}).

(5) To avoid correction for baseline drift, measurements of the displacement at zero flow condition, before and after the measurement, are compared. The measurement is rejected when the difference between the observation is not within 1% of the observed mean value.

(6) Recalibration of the hot wire after an observation series. The series is rejected if the difference with the first calibration is more than 2%.

4. Results

4.1. *Measurement of the turbulent boundary layer*

The profiles of the mean velocity and the velocity fluctuations have been measured at five different wind tunnel speeds at a position 1 cm behind the lift force sensor.

In the near-wall region the mean velocity profile is usually expressed in terms of the so-called law of the wall (see e.g. Monin & Yaglom 1973; Hinze 1975), which reads

$$u^+ = f(y^+) \tag{4.1}$$

where the $y^+ = yu_*/\nu$ and $u^+ = u/u_*$. The friction velocity, u_*, is defined as

$$u_* = \left(\frac{\tau_0}{\rho}\right)^{0.5} \tag{4.2}$$

with τ_0 the surface shear stress.

It is well established that the turbulent boundary layer near a wall can be divided into three regions (Hinze 1975; Tennekes & Lumley 1972): the viscous sublayer ($0 < y^+ < 5$), the buffer layer ($5 < y^+ < 30$) and the logarithmic layer ($y^+ > 30$).

We have used the logarithmic part of the measured velocity profile to calculate the friction velocity by fitting the data points to the expression:

$$u^+ = 2.44 \ln y^+ + 4.9. \tag{4.3}$$

We estimate that the accuracy of the friction velocity determined in this way is 2%. Its value as a function of the free-stream velocity, u_0, is given in table 2. It is not possible to calculate the friction velocity directly from the linear profile valid near the wall (see figure 4). First, the hot-wire anemometer could not be calibrated with sufficient accuracy at the low velocities which occur in this region. Second, a hot-wire anemometer in close proximity to the wall ($y^+ < 3$), suffers from enhanced cooling so that an apparently higher velocity is measured than in reality, as is apparent in figure 4. As a result, only a limited number of points could be measured in the viscous sublayer with reasonable accuracy and these are not sufficient to determine the friction velocity. Nevertheless, it seems that in the limited region where reliable hot-wire measurements could be made, i.e. between $3 < y^+ < 5$, the observations scaled with u_*, obtained according to the procedure mentioned above, fit very closely to the linear profile valid in the viscous sublayer profile and this gives confidence in our estimate of u_*.

u_0(m s^{-1})	u_*(m s^{-1})	Re_x	δ^*(cm)	θ(cm)	H
4.28	0.185	8.56×10^6	0.8783	0.6224	1.411
6.44	0.268	1.29×10^6	0.7996	0.5762	1.388
8.71	0.352	1.74×10^6	0.7340	0.5271	1.393
10.70	0.420	2.14×10^6	0.7262	0.5273	1.377
12.34	0.477	2.48×10^6	0.7375	0.5369	1.374

TABLE 2. Free-stream velocity and corresponding friction velocities based on the logarithmic boundary layer.

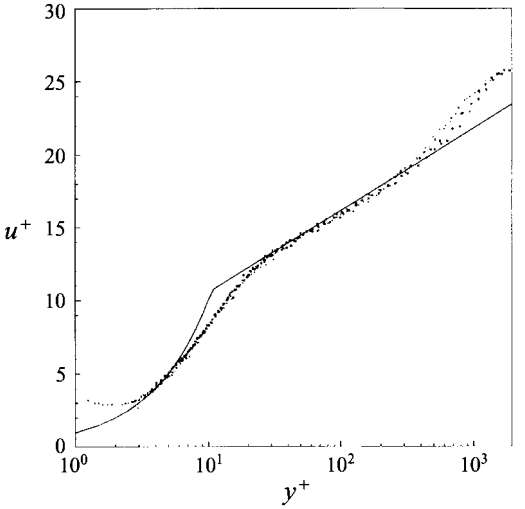

FIGURE 4. Boundary layer profile, velocity *vs.* distance in dimensionless form. Free-stream velocities: 4.28, 6.44, 8.71, 10.70, 12.34 m s^{-1}. The solid curve shows the law of the wall.

The results for the mean velocity are shown in figure 4 and the measured velocities collapse very well on the law of the wall mentioned above. Other relevant parameters can be obtained from the mean velocity profile as a function of the Reynolds number

$$Re_x = \frac{u_0 x}{\nu} \tag{4.4}$$

where the distance, x, is measured from the leading edge of the plate to the lift force sensor. These parameters are the displacement thickness

$$\delta^* = \int_0^\infty \left(1 - \frac{u}{u_0}\right) \mathrm{d}y, \tag{4.5}$$

and the momentum thickness

$$\theta = \int_0^\infty \frac{u}{u_0}\left(1 - \frac{u}{u_0}\right) \mathrm{d}y. \tag{4.6}$$

Since the hot wire could not be used below $y^+=3$, the velocity profile in the range $0 < y^+ < 3$ is obtained by extrapolation with the help of a linear profile. From these parameters one may calculate the shape factor as

$$H = \frac{\delta^*}{\theta}. \tag{4.7}$$

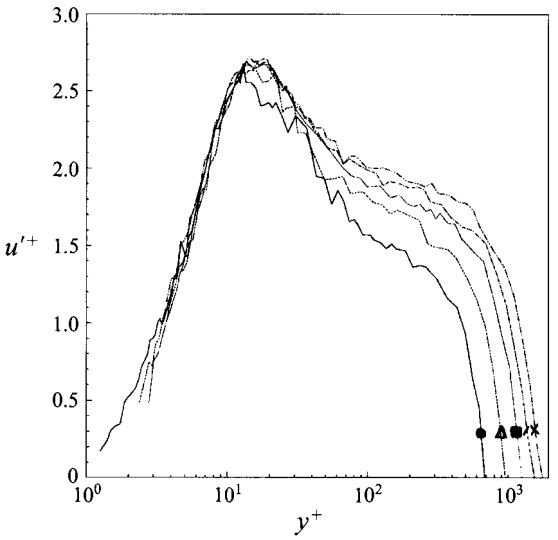

FIGURE 5. Velocity fluctuations as a function of the distance in dimensionless form. Free-stream velocity in m s^{-1}: •, 4.28 m s^{-1}; △, 6.44 m s^{-1}; ■, 8.71 m s^{-1}; /, 10.70 m s^{-1}; x, 12.34 m s^{-1}.

From the literature it is known that in the case of a zero pressure gradient $H \approx 1.4$ (see Hinze 1975, p. 633). From the experimental values given in table 2 we find $H = 1.389 \pm 0.014$.

With the data of table 3 the following relationship between the free-stream velocity and the friction velocity is found:

$$u_* = ((33.23 \pm 4.6) + (36.18 \pm 0.51)\, u_0)\, 10^{-3}. \tag{4.8}$$

Uncertainties in the measurement of the temperature (density and viscosity of the air) are taken in to account in this equation.

The standard deviation of the horizontal velocity fluctuations is shown in figure 5. The measurements scaled in terms of the characteristic wall parameters collapse on a single profile, especially near the wall ($y^+ < 10$). The maximum value of $u^+=2.6$ at $y^+=11$ agrees with other the measurements. e.g. given by Monin & Yaglom (1973) and by Durst, Jovanovic & Sender (1993). For larger values of the dimensionless distance the velocity fluctuations decrease until they go rapidly to zero around $y^+=500$, i.e. near the edge of the boundary layer. The exact dimensionless distance at which the velocity fluctuations approach zero depends on the boundary layer thickness, which is a function of Reynolds number based on the length of the plate (see figure 5).

The particles that we consider, are always smaller than the depth of the viscous sublayer, i.e. the dimensionless radius $a^+ < 5$. This corresponds with almost all real entrainment situations. For instance, a sand particle on a flat surface with a diameter of 200 μm lies within the viscous sublayer if the free wind velocity over the particle does not exceed 8 m s^{-1}. From its name 'viscous sublayer' one would perhaps expect the dynamics of this layer to be dominated by viscous effects. However, the contrary is true. The flow characteristics within the viscous sublayer are largely determined by the turbulence in the boundary layer, especially the buffer layer. As a result one finds in the surface layer large organized flow structures, i.e. larger than a viscous length scale. Examples are so-called low-speed streaks (Kline *et al.* 1967) and streamwise vortices (Brooke & Hanratty 1993; Hamilton, Kim & Waleffe 1995). It has been

found that flow properties in the viscous sublayer, such as the wall shear stress, are highly fluctuating (Chew, Khod & Li 1994 and Obi *et al.* 1995). The observations lead to a skewness factor of these wall shear stress fluctuations of around 1 and a kurtosis of around 5. These fluctuations must clearly have an influence on the force on a particle in the viscous sublayer. In particular one should expect this force to be strongly fluctuating.

Finally, we note that any influence of the lift force sensor with the particle on the velocity measurement could not be detected. This seems quite reasonable because a particle smaller than the thickness of the viscous sublayer does not disturb the boundary layer so that the wall remains aerodynamically smooth. The velocity profiles measured 1 cm before and after the lift force sensor give the same results within 0.5%. Horizontal traverses at these positions also show that the flow is uniform in the lateral direction as has been already mentioned in §2. It is, however, possible that the particle and lift force sensor influence the local velocity profile very close to the wall ($y^+ < 3$), but this could not be investigated with the present hot-wire anemometer. We were also not able to determine an influence of the gap below the particle (see figure 1) on the lift force but we consider such influence unlikely since the measurement with no particle led to a zero force. We attempted to measure the influence of the gap on the flow profile by making vertical traverses through the boundary layer at several position before and after the cantilever. However no influence on the velocity profile could be detected.

4.2. *Lift force*

4.2.1. *Measurement of the mean lift force*

The observed values of the lift force F are presented in dimensionless form (F^+) given by

$$F^+ = \frac{F}{\rho \nu^2} \tag{4.9}$$

where dimensionless particle radius a^+ is defined as

$$a^+ = \frac{a u_*}{\nu}. \tag{4.10}$$

For the main set of experiments we have used the hollow glass sphere. The duration of each experiment is approximately 5 minutes. A measurement run is started at zero speed. The wind tunnel is turned on and the free-stream velocity is increased until it reaches that at which the observation of the lift force is to be taken. This velocity is kept constant for two minutes after which the wind tunnel is turned off. The reading of the lift sensor at the start and end of the run, i.e. at zero velocity, is used as a quality indicator of the measurement, following the requirement mentioned in §3. The advantage of performing a measurement at a single velocity is that the duration of each individual measurement is rather short so that fewer experiments have to be rejected because of baseline drift of the lift force measuring device. The results of the measurements are given in figure 6. Each data point displayed is the average value of 200 independent observations made during one run. Each observation is the average over 0.1 s of continuous measurement at 50 kHz. The data points in figure 6 have been fitted with a power law using a logarithmic least-squares method and imposing $F_L^+=0$ at $a^+=0$. The result with correlation coefficient of 0.962 reads

$$F_L^+ = (56.9 \pm 1.1)(a^+)^{1.87 \pm 0.04}. \tag{4.11}$$

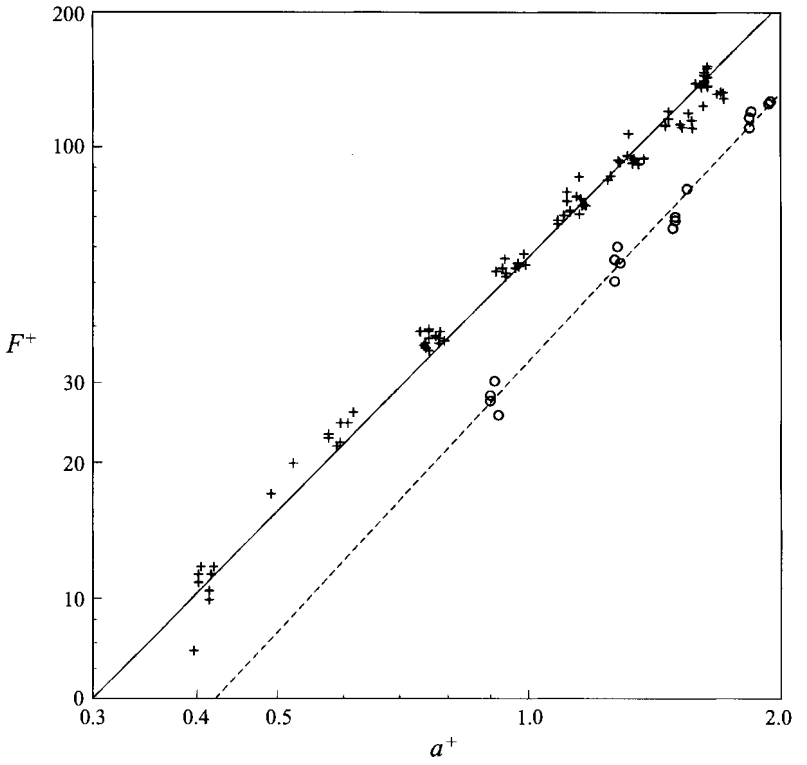

FIGURE 6. Dimensionless lift force as a function of the dimensionless radius: +, hollow particle ($d_p = 120$ μm); ○, plastic particle ($d_p = 218$ μm); —, $F_L^+ = 56.9(a^+)^{1.87}$; - - -, $F_L^+ = 33.4(a^+)^{1.98}$.

An attempt to measure the lift force at a larger dimensionless radius by increasing the wind tunnel speed has not been successful. We found that for velocities above 16 m s^{-1} the measured mean lift force becomes almost constant. This is due to the fact that the cantilever reaches its maximum upward deflection of about 2 μm at a value of $a^+ = 2$ or at a value of $F_L^+ \approx 200$.

Another attempt to measure at a larger a^+ by using the larger plastic particle was also not successful. As could be expected the cantilever again reaches its maximum deflection at a dimensionless radius of 2. Another problem with this particle is that the resonance frequency mentioned in §2 is lower due to the larger weight of the particle and it falls in the range of turbulent fluctuations. Nevertheless, some observations at higher values of a^+ could be made. The following relationship between the dimensionless radius and the lift force is found with a correlation coefficient of 0.987:

$$F_L^+ = (33.4 \pm 3.0)(a^+)^{1.98\pm0.06}, \tag{4.12}$$

which is also shown in figure 6.

It is however doubtful whether this measurement is completely reliable. Sources of possible errors are the very low resonance frequency of this system (200 Hz) and the initial downward bending of the cantilever due to the weight of the massive particle. The offset compensating the initial downward bending due to the weight of the heavy particle ($\approx 8 \times 10^{-8}$N) is larger than the displacement due to the mean lift force ($\approx 10^{-8}$N). Moreover, the larger contact area of the solid particle with the cantilever may cause an increased stiffness of the system. This would for instance explain the

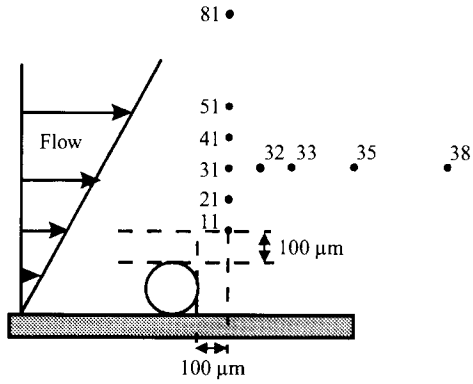

FIGURE 7. The solid circles indicate the positions of the sensitive element of the hot-wire anemometer relative to the particle. First digit is vertical displacement in 100 μm, second digit is horizontal displacement in 100 μm, e.g. 32 means 300 μm above and 200 μm behind the particle.

smaller coefficient in (4.12) with respect to the coefficient found in (4.11). However, we note that the experiments performed with both spheres lead to quite similar values for the exponent in the power law.

4.2.2. *Measurement of the fluctuating lift force*

Our sensor also allows measurement of the fluctuating lift force. These fluctuations may be important for entrainment of particles, because the extreme values of the lift force are primarily responsible for particle detachment from the wall. For these measurements, the data gathered from the hot-wire anemometer and from the lift force sensor, were recorded with a frequency of 50 kHz for a period of 5 s. For the experiments we use the hollow glass particle, the hot wire anemometer is placed at a number of different positions relative to the particle, as shown in figure 7. The hot-wire anemometer is always placed downstream of the particle since the relatively large prongs which hold the hot wire may introduce an unwanted disturbance of the flow near the particle and the lift force sensor. The lift force and the velocity statistics are measured at four different free-stream velocities (4.0, 6.0, 9.0, and 12.0 m s^{-1}) and at six vertical positions of the hot wire, i.e. positions 11, 21, 31, 41, 51, and 81. The lift force and the velocity statistics at the horizontal positions 31, 32, 33, 35, and 38 of the hot-wire anemometer are measured at three different velocities (4.0, 6.0, and 9.0 m s^{-1}).

Figure 8 shows the probability curves of the dimensionless velocity, u^+, at the various vertical positions of the hot-wire anemometer and at the four free-stream velocities mentioned above. In figure 9 we depict the corresponding probability curves for the dimensionless lift force, F_L^+. In both cases the values of the fluctuations are normalized with the mean value and the standard deviation.

The probability curves of the velocity show that the shape of the velocity distribution varies weakly with the distance to the wall. The shape of the probability distribution of the lift force fluctuations is approximately constant as function of the hot-wire position (except for the lowest position), consistent with no influence by the hot wire on the lift force measurements.

The statistical quantities of the dimensionless velocity fluctuations at all measurement positions (i.e. at the several horizontal and vertical positions of the hot-wire anemometer) are given in table 3. From the data, it can be noted that there is a

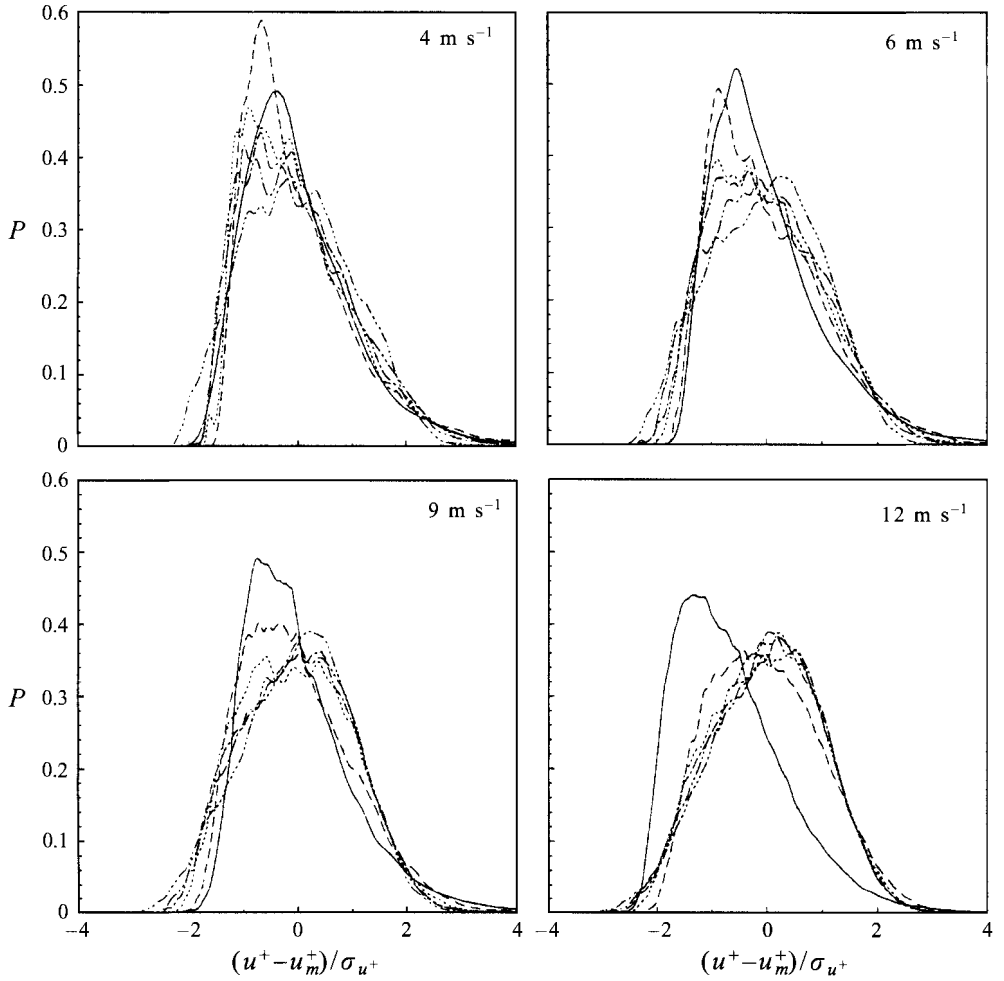

FIGURE 8. Probability curves of the dimensionless velocity for a number of different free-stream velocities and vertical positions of the hot-wire anemometer: ——, 11; — —, 21; – –, 31; —·—, 41; —··—, 51; —···—, 81.

significant difference between the measurements at the first horizontal position (31) and the other positions (32, 33, 35, 38). This is caused by an error in the positioning of the traversing mechanism for the hot-wire anemometer. The velocity is first measured at the vertical positions (11, 21, 31, 41, 51, 81) and then at the horizontal positions (32, 33, 35, 38). It is difficult to reposition the hot wire at the same height above the plate as the first point (31). This difference could be as large as 50 μm which explains the differences found in table 4.

Comparing our results for the velocity statistics with the DNS data of Spalart (1988) and the experimental data of Ching, Djenide & Antonia (1995), we find good agreement for the mean velocities. Our results for the r.m.s. values are somewhat smaller than the results obtained from the other data sets. This is most probably due to the averaging due to the hot-wire length of 0.5 mm. Our results together with the observed probability functions of the lift force, allow us to conclude that at low free-stream velocities, the lift force is possibly slightly influenced by presence of

Pos. of hot wire	y^+	u^+ mean	u^+ mod.	Stand. dev.	Skewness	Kurtosis
			Free-stream velocity 4.0 m s^{-1}			
11	2.84	2.84	2.80	0.29	1.32	6.38
21	3.71	3.71	3.49	0.84	1.31	5.11
31	4.79	4.79	4.56	1.37	1.08	4.58
41	5.95	5.87	5.58	1.68	0.69	3.11
51	7.04	6.71	6.48	1.95	0.63	2.99
81	11.22	9.04	8.97	2.30	0.17	2.40
32	3.84	3.84	3.62	0.95	1.40	5.65
33	3.86	3.86	3.66	0.96	1.15	4.41
35	4.06	4.06	3.85	0.99	1.09	4.30
38	4.30	4.30	4.09	1.10	1.17	4.75
			Free-stream velocity 6.0 m s^{-1}			
11	3.03	3.03	2.90	0.60	1.304	5.72
21	5.09	5.09	4.76	1.58	0.819	3.39
31	7.37	6.89	6.64	2.08	0.528	2.79
41	9.38	8.15	7.93	2.29	0.397	2.58
51	11.79	9.29	9.20	2.49	0.237	2.48
81	17.54	11.27	11.33	2.56	−0.038	2.33
32	5.68	5.63	5.32	1.83	0.722	3.19
33	5.51	5.48	5.27	1.71	0.721	3.35
35	5.82	5.76	5.55	1.73	0.607	3.00
38	6.36	6.20	5.93	1.82	0.708	3.24
			Free-stream velocity 9.0 m s^{-1}			
11	3.35	3.35	3.18	0.91	1.255	5.62
21	6.45	6.27	6.02	1.98	0.644	3.10
31	9.61	8.27	8.17	2.37	0.253	2.46
41	12.37	9.53	9.51	2.44	0.092	2.40
51	15.14	10.54	10.58	2.50	0.048	2.44
81	21.79	12.36	12.48	2.39	−0.129	2.59
32	9.35	8.12	8.04	2.30	0.236	2.48
33	9.35	8.13	8.04	2.27	0.244	2.53
35	9.53	8.22	8.10	2.35	0.228	2.40
38	9.97	8.45	8.31	2.24	0.264	2.44
			Free-stream velocity 12.0 m s^{-1}			
11	5.60	5.56	4.29	1.53	0.941	4.08
21	9.38	8.14	7.94	2.41	0.355	2.59
31	15.66	10.71	10.75	2.59	0.070	2.44
41	20.43	12.04	12.16	2.61	−0.051	2.45
51	24.13	12.87	12.94	2.53	−0.088	2.56
81	31.63	14.22	14.33	2.33	−0.099	2.70

TABLE 3. Statistical quantities for the dimensionless velocity.

the hot-wire anemometer; at the higher free-stream velocities there is, however, no measurable influence.

From the data on the skewness and the kurtosis of the dimensionless velocity fluctuations, given in table 3, it follows that very close to the wall the probability curve is somewhat skewed to the right and is sharper than a normal distribution. Farther away from the surface the skewness decreases and the distribution approaches a Gaussian distribution. This agrees at least qualitatively with other results which are primarily obtained from DNS. However, we should again mention here that the hot-wire anemometer cannot be very well calibrated at low velocities, and at low

Pos. of hot wire	F_L^+ (mod.-mean)	Stand. dev.	Skewness	Kurtosis
Free-stream velocity 4.0 m s^{-1}, u_*=0.18 m s^{-1}, a^+=0.71, F_L^+=30.1				
11	−0.688	14.80	0.034	3.43
21	−0.937	14.52	0.318	3.22
31	−0.169	12.02	0.490	4.97
41	−0.685	9.13	0.313	3.62
51	−0.281	9.10	0.460	3.79
81	−0.810	8.68	0.556	4.53
32	−0.490	10.50	0.366	3.65
33	−0.621	9.03	0.394	3.68
35	−0.594	8.51	0.364	3.82
38	−0.069	8.63	0.398	3.82
Free-stream velocity 6.0 m s^{-1}, u_*=0.25 m s^{-1}, a^+=1.00, F_L^+=57.0				
11	−2.15	22.80	0.895	5.46
21	−2.51	21.94	0.893	5.01
31	−2.61	19.77	1.003	5.58
41	−2.58	18.48	1.213	6.96
51	−2.12	18.33	1.128	6.32
81	−1.56	17.32	1.304	8.17
32	−2.05	19.66	0.971	5.40
33	−2.57	18.09	1.240	7.02
35	−2.16	17.34	1.203	7.12
38	−2.89	18.31	1.421	8.33
Free-stream velocity 9.0 m s^{-1}, u_*=0.36 m s^{-1}, a^+=1.44, F_L^+=111.9				
11	−6.77	43.87	0.905	5.12
21	−6.37	44.24	0.929	5.57
31	−6.33	43.36	0.890	4.97
41	−5.95	42.84	0.949	5.13
51	−6.60	43.15	1.044	5.47
81	−6.38	43.14	0.998	5.01
32	−6.99	43.63	1.039	5.55
33	−6.19	42.20	1.004	5.58
35	−6.76	42.57	1.015	5.42
38	−6.18	40.05	1.079	5.65
Free-stream velocity 12.0 m s^{-1}, u_*=0.47 m s^{-1}, a^+=1 87, F_L^+=183.3				
11	−4.13	107.23	−0.0536	3.19
21	−4.73	103.12	0.0088	3.11
31	−4.17	104.49	−0.0461	3.17
41	−4.28	103.84	−0.0044	3.13
51	−4.79	108.73	−0.0032	3.08
81	−4.93	108.98	0.0140	3.07

TABLE 4. Statistical quantities of the dimensionless lift force F_L^+ is taken from equation (4.11).

heights is also influenced by the presence of the wall. These effects will in particular influence the higher-order moments.

In table 4 we present the statistics for the dimensionless lift force fluctuations. First we note that the standard deviation of the lift force fluctuations is in all cases significantly larger than the r.m.s. data given in table 1 which show results for when there is no particle attached to the cantilever and when the lift force sensor is shielded from the air flow by a cover. So the lift force fluctuations can be attributed to the velocity fluctuations in the viscous sublayer. This conclusion seems to be corroborated by the fact that the standard deviation of the fluctuations becomes larger when the

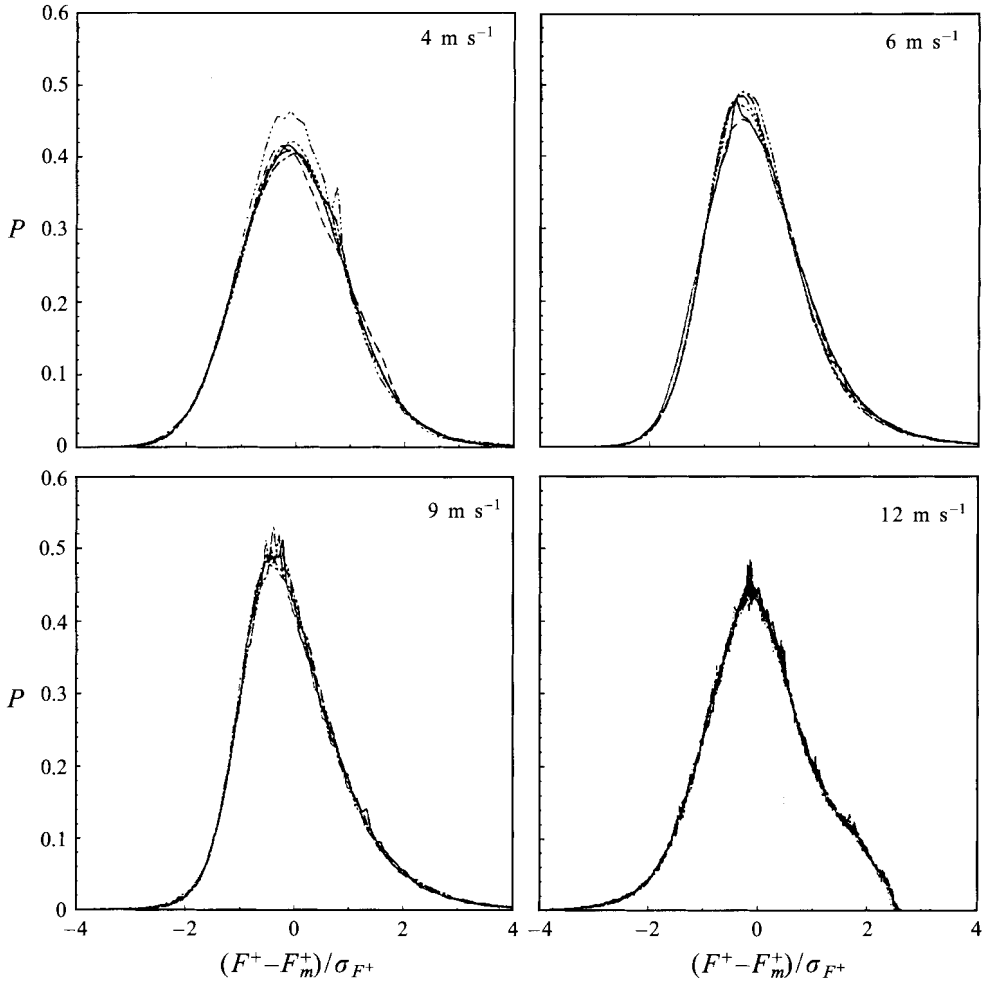

FIGURE 9. Probability curves of the dimensionless lift force for a number of different free-stream velocities and vertical positions of the hot-wire anemometer: ——, 11; — —, 21; – –, 31; —·—, 41; —··—, 51; —···—, 81.

free-stream velocity increases. Note that the measurement of the displacement of the cantilever, and thus of the fluctuating component of the lift force, taken at the highest velocities is influenced by the contribution of the resonance of the cantilever.

Figure 9 and table 4 suggest that the probability distribution of the lift force is non-Gaussian with a positive skewness and a kurtosis larger than 3. The data taken at the free-stream velocities, u_0=6 and 9 m s^{-1}, lead to values of approximately 1 and 5 for the skewness and the kurtosis, respectively. These values agree reasonably well with the data for the same velocity statistics taken at the lowest hot-wire measuring position as given in table 3 and also with the statistics of the wall shear stress measurements taken by Obi *et al.* (1995) as mentioned in §4.1. This suggests that the lift force is indeed caused be the fluctuating velocity shear near the surface.

For the highest velocity we observe a much lower values for the skewness and the kurtosis. This may be explained by the fact that in this case the highest lift force

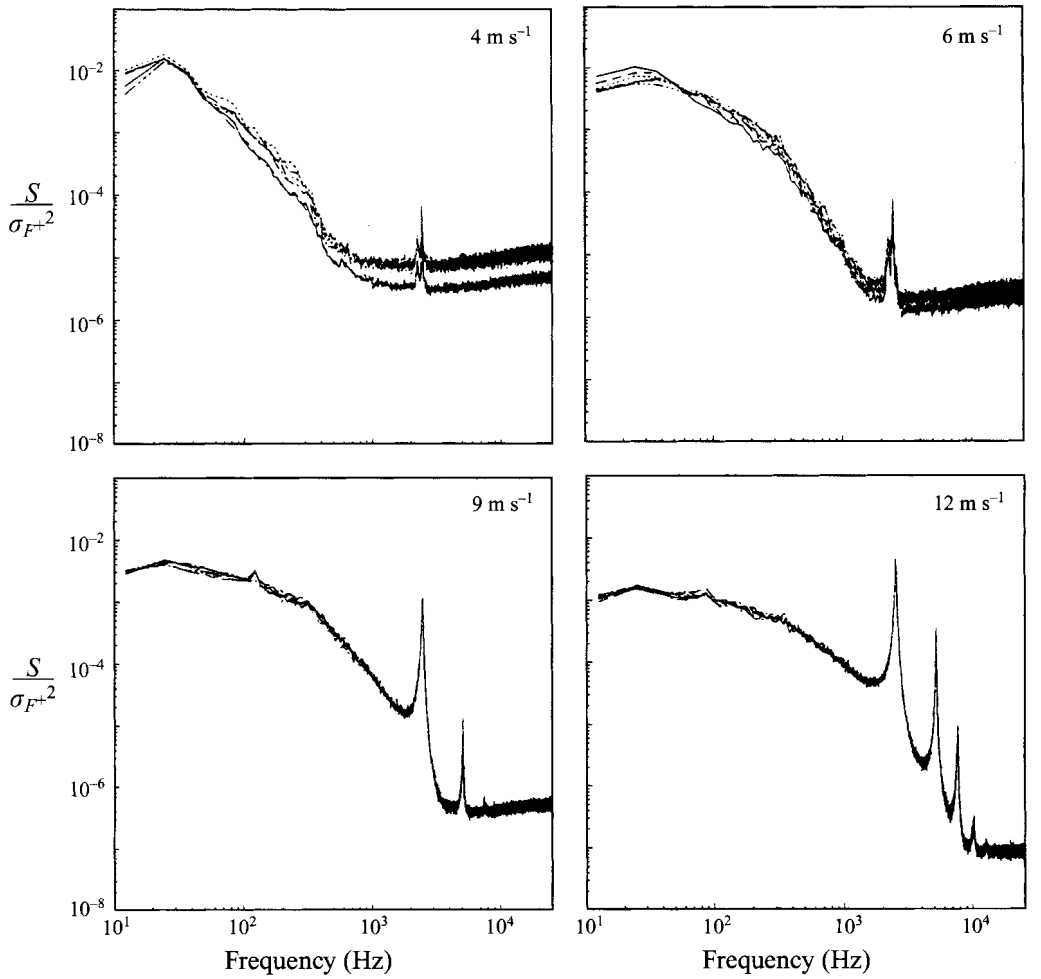

FIGURE 10. Power spectra of the dimensionless lift force for a number of different free-stream velocities and vertical positions of the hot wire anemometer: ——, 11; — —, 21; – –, 31; —·—, 41; —··—, 51; —···—, 81.

fluctuations will be limited by the maximum upward deflection of the cantilever. Furthermore, the resonance to be discussed below may also play a role.

In figure 10 the power spectra of the dimensionless lift force fluctuations are shown as a function of the free-stream velocity and the vertical positions of the hot wire. In each case the spectrum has been scaled with the variance. The spectra for the velocity fluctuations appear quite standard and will not be shown; they may be found in Mollinger (1995).

These power spectra show that as a function of mean velocity the effect of the resonance vibration discussed in §2 increases where the resonance was already. The contribution of the resonance peaks for mean velocities smaller than 6 m s^{-1} is smaller than 0.5%, for 9 m s^{-1} it is 5.5% and for 12 m s^{-1} it is 29% of the total standard deviation. This clearly confirms our doubts, already referred to above, the measurements taken at the highest velocity. The resonance frequency and its higher harmonics appear to be 2.5, 5.0, and 10.0 kHz. The peak in figure 10 at about 7.5 kHz for the highest free-stream velocity, i.e. 12 m s^{-1}, is probably due to interference of

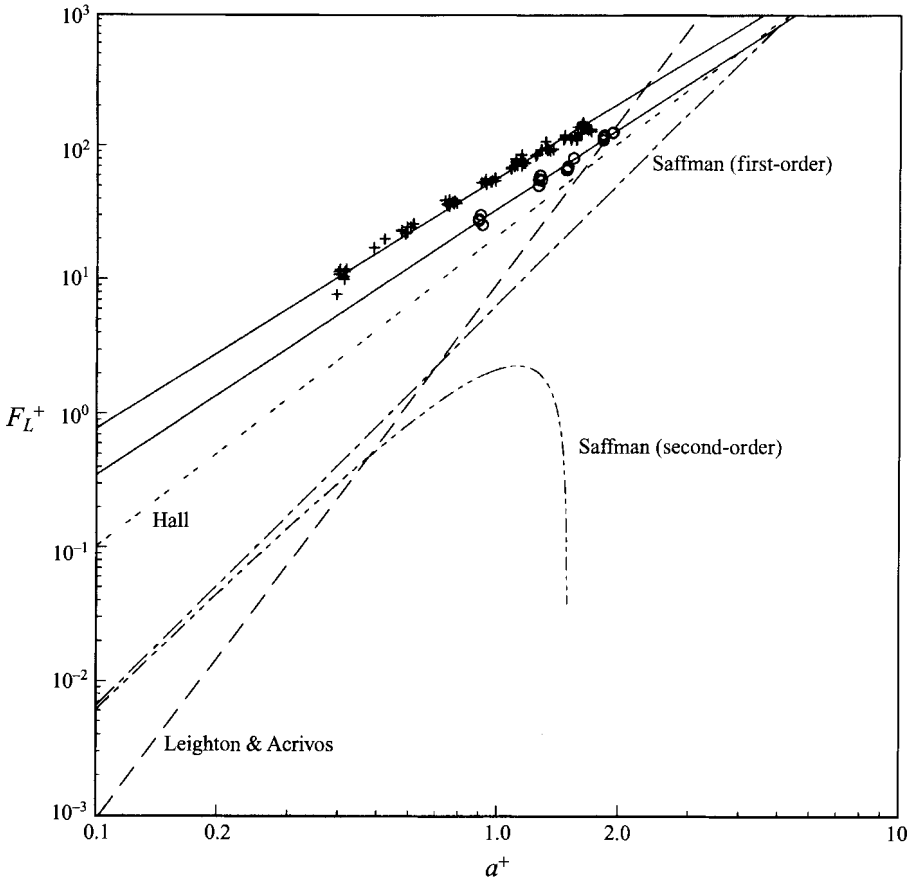

FIGURE 11. Lift force as a function of the dimensionless radius. +, $F_L^+ = 56.9(a^+)^{1.87}$ (eq. (4.11), exp.); ○, $F_L^+ = 33.4(a^+)^{1.98}$ (eq. (4.12), exp.); Saffman: first-order (1965) $F_L^+ = 6.46(a^+)^3$ (eq. (5.1), th.); second-order $F_L^+ = 6.46(a^+)^3 - 4.32(a^+)^4$ (eq. (1.3), th.); Leighton & Acrivos (1985) $F_L^+ = 9.22(a^+)^4$ (eq. (5.2), th.); Hall (1988) $F_L^+ = 20.9(a^+)^{2.31}$ (eq. (5.3), exp.).

the first two resonance peaks. The resonance vibrations are nevertheless far less pronounced than the ones which occur when the large (heavy) particle is used.

5. Comparison with theory and other observations

As discussed in the introduction, a theoretical treatment of the equations of motion which is valid for a sphere on a surface in a linear shear flow (with $1 < a^+ < 10$) and which can be used to calculate the lift force has not been achieved yet. Nevertheless it is interesting to compare our measurements with a number of theoretical expressions valid at lower values of a^+.

In figure 11 our experimental data are plotted together with the theoretical expressions which were discussed in the introduction. Again, it has to be stressed that these theoretical results are derived under the assumption that $a^+ \ll 1$, whereas in the experiments $a^+ \approx 1$. First, these expressions are rewritten in a dimensionless form using the friction velocity (u_*) and the kinematic viscosity (ν). Using $V = a\kappa$ and

$u_*^2 = \nu\kappa$, we find for the expressions of Saffman (1965)

$$F_L^+ = 6.46(a^+)^3. \tag{5.1}$$

The expression of Leighton & Acrivos (1985) in dimensionless form reads

$$F_L^+ = 9.22(a^+)^4. \tag{5.2}$$

In addition we plot in figure 11 the experimental data on the lift force obtained by Hall (1988). Put in non-dimensionless form they are

$$F_L^+ = 20.9(a^+)^{2.31}. \tag{5.3}$$

We should emphasize here that the data of Hall were obtained for $a^+ > 3$. Nevertheless, the power law (5.3) has an exponent close to the value found with our results. As a result we feel able to conclude that the value of the exponent in the power law that describes the lift force, F_L^+ as function of a^+, seems to lie close to 2. In contrast, the theoretical expressions (5.1) and (5.2) for F_L^+ predict higher exponents, i.e. 3 or even 4.

The dependence of the lift force on $(a^+)^2$ may be tentatively explained by the following simple dimensional argument. Let us assume that in the region near $a^+=1$ viscous forces are still important (for $a^+=1$ the viscous and the inertia forces are of the same order since a^+ is a Reynolds number), but that the fundamental property of Stokes flow, i.e. time reversibility, is no longer appropriate. In that case we would expect that the only parameters of influence are a, ν and $\mathrm{d}u/\mathrm{d}y$. In other words the inertial forces are assumed to be negligible so the density drops from the parameter list. Based on this choice of characteristic parameters it then follows by dimensional analysis that $F_L \sim \rho\nu a^2 \partial u/\partial y$ which in dimensionless form leads to $F_L^+ \sim (a^+)^2$. The higher power of F_L^+ in terms of a^+ in (5.1) and (5.2) follows from the fact that in the Stokes limit $F \sim a^2$ cannot exist because of time reversibility (i.e. the coefficient in a series expansion of F_L^+ in terms of a^+ becomes identically zero for the quadratic term) and thus higher-order terms (which include inertia) must be taken into account. Our results imply that at $a^+ \approx 1$ the quadratic term can no longer be neglected.

As another possible explanation for the discrepancy between theory and experiment, we note again that the velocity in the viscous sublayer is highly non-stationary, whereas the solutions of the Stokes flow are by definition valid for stationary flow. This non-stationary behaviour can influence the lift force in an unknown way, e.g. by non-stationary vorticity diffusion (Lovalenti & Brady 1995).

Only the measurements of Hille *et al.* (1982) and Radecke & Schulz-Dubois (1988) provide some additional data on the fluctuating component of the lift force, but only for relative large Reynolds numbers ($O(100)$). Nevertheless, their results suggest that the probability curve of the lift force is skewed more to the right (positive skewness) as the velocity increases, which is consistent with our experiments.

6. Summary and conclusion

A novel experimental set-up has been developed and built with which it is possible to measure the mean and the fluctuating lift force on a small sphere (diameter about 100 μm) fixed on a flat plate and embedded in the viscous sublayer of a turbulent boundary layer. The sphere is attached to a flexible silicium cantilever placed flush to the measuring plate in such a way that only the particle protrudes into the viscous sublayer. The deflection of the cantilever, which is a measure of the lift force, is accurately measured with an optical focus detection system.

The data for the lift force were obtained in a turbulent boundary layer for $0.3 < a^+ < 2$. The mean lift force seems to follow the relationship:

$$F_L^+ = (56.9 \pm 1.1)(a^+)^{1.87\pm0.04}. \tag{6.1}$$

This result for this lift force is rather close, as far as the exponent is concerned, to the results obtained by Hall (1988) who used a quite different experimental set-up.

Experiments performed with a larger sphere also follow a power law with a similar exponent but with a slightly smaller coefficient. However, owing to several problems, we consider this latter experiment as less trustworthy.

In all cases the exponent of the power law is close to 2, which implies that the mean dimensionless lift force is proportional to $(a^+)^2$. This is in contradiction with theoretical results based on Stokes flow valid for very small values of a^+, which predict $F_L^+ \sim (a^+)^4$.

The measurements of the fluctuating lift force give a distribution which is positively skewed, i.e. to large positive values, and has a kurtosis larger than 3. This means that the particle occasionally experiences a very large positive lift forces, which e.g. may lead to lift up and consequently to entrainment in the flow. The values of the skewness and kurtosis agree reasonably well with the same statistics obtained from near-wall velocity measurements and from wall-shear stress measurements. This suggests that the lift force is indeed related to the velocity shear.

The authors are grateful for the ideas generated, and the support given by J. M. Bessem, R. v.d. Boom and H. Leijdens from the Delft University of Technology. We thank Cor Gerritse and Anton Haaring for their help in constructing the experimental set-up. The CD-player system was generously provided by W.G. Ophey of the Philips Research Laboratories, Eindhoven, The Netherlands. This work was financially supported by the 'Stimuleringsruimte' of the Delft University of Technology under project number 89-STM-S-8.

REFERENCES

BAGNOLD, R. A. 1961 *The Physics of Blown Sands and Desert Dunes.* Chapman & Hall.

BAGNOLD, R. A. 1974 Fluid forces on a body in shear flow; experimental use of stationary flow. *Proc. R. Soc. Lond.* A **340**, 147–171.

BOUWHUIS, G., BRAAT, J., HUYSER, A., PASMAN, J., ROSMALEN, G. VAN & SCHOUHAMER-IMMINK, K. 1985 *Principles of Optical Disc Systems.* Adam Hilger.

BROOKE, J. W. & HANRATTY, T. J. 1993 Origin of turbulence-producing eddies in a channel flow *Phys. Fluids* A **5**, 1011–1022.

CHERUKAT, P. & MCLAUGHLIN, J. B. 1994 The inertial lift on a rigid sphere in a linear shear flow field near a wall. *J. Fluid Mech.* **263**, 1–18.

CHEW, Y.T., KHOO, B. C. & LI, G. L. 1994 A time resolved hot-wire sensor shear stress probe for turbulent flow: use of laminar flow calibration. *Exps. Fluids* **17**, 75–83.

CHING, C. Y., DJENIDI, L. & ANTONIA, R. A. 1995 Low-Reynolds-number effects in a turbulent boundary layer. *Exps. Fluids* **16**, 61–68.

DURST, F., JOVANOVIC, J. & SENDER, J. 1994 Detailed measurements of the near wall region of a turbulent pipe flow. In *Data Validation of Cfd Codes* (ed. D. Goldstein, D. Hughes, R. Johnson & D. Lankford). ASME-FED, Vol. 146.

EICHHORN, R. & SMALL, S. 1964 Experiments on the lift and drag of spheres suspended in a Poiseuille flow. *J. Fluid Mech.* **20**, 513–527.

HALL, D. 1988 Measurements of the mean force on a particle near a boundary in turbulent flow. *J. Fluid Mech.* **187**, 451–466.

HAMILTON, J. M., KIM, J. & WALEFF, F. 1995 Regeneration mechanisms of near-wall turbulence structures. *J. Fluid Mech.* **287**, 317–348.

HILLE, P., MAGENS, E. & TESSMER, W. 1982 Forces on a single sediment grain and their dependence on the surrounding flow field. *Euromech 156: Mechanics of Sediment Transport. Istanbul*, pp. 73–77.

HINZE, J. O. 1975 *Turbulence*. McGraw-Hill.

JEFFREYS, H. 1929 On the transport of sediments by streams. *Proc. Camb. Phil. Soc.* **25**, 272–276.

KLINE, S. J., REYNOLDS, W. C., SCHRAUB, F. A. & RUNDSTADLER, P. W. 1967 The structure of turbulent boundary layers. *J. Fluid Mech.* **30**, 741–773.

LEIGHTON, D. & ACRIVOS, A. 1985 The lift on a small sphere touching a plane wall in the presence of a simple shear flow. *Math. Phys. Z.Angew.* **36**, 174–178.

LOVALENTI, P. M. & BRADY, J. F. 1995 The temporal behaviour of the hydrodynamic force on a body in response to an abrupt change in velocity at small but finite Reynolds number. *J. Fluid Mech.* **293**, 35–46.

MCLAUGHLIN, J. B. 1989 Aerosol deposition in numerically simulated channel flow. *Phys. Fluids* A **1**, 1211–1224.

MCLAUGHLIN, J. B. 1991 Inertial migration of a small sphere in linear shear flows. *J. Fluid Mech.* **224**, 261–274.

MCLAUGHLIN, J. B. 1993 The lift on a small sphere in wall-bounded linear shear flows. *J. Fluid Mech.* **246**, 249–265.

MOLLINGER, A. M. 1995 Particle Entrainment, measurement of the fluctuating lift force. PhD thesis, Delft University of Technology.

MOLLINGER, A. M., NIEUWSTADT, F. T. M. & BESSEM, J. M. 1995 A new device to measure the lift on a particle in the viscous sublayer. *Measurement Sci. Technol.* **6**, 206–213.

MONIN, A. S. & YAGLOM, A. M. 1973 *Statistical Fluid Mechanics, Mechanics of Turbulence*, Vol. 1. MIT Press.

OBI, S., INOUE, K., FURUKAWA, T. & MASUDA, S. 1995 Experimental study on the statistics of wall shear stress in turbulent channel flow. *Proc. 10th Symp. Turbulent Shear Flows. The Pennsylvania State University, August 14–16*, pp. 5.19–5.24.

PARK SCIENTIFIC 1992 *Instruments Technical Bulletin*. Sunnyvale, CA, USA.

PHILLIPS, M. 1980 A force balance model for particle entrainment onto a fluid stream. *J. Phys.* D: *Appl. Phys.* **13**, 221–233.

RADECKE, H. VAN & SCHULZ-DUBOIS, E. O. 1988 Linear response of fluctuating forces to turbulent velocity components. In *Applications of Laser Anemometry to Fluid Mechanics. 4th Intl. Symp., Lisbon, Portugal* (ed. R. J. Adrian), pp. 23–44. Springer.

ROSENTHAL, G. N. & SLEATH, J. F. A. 1986 Measurement of lift in oscillatory flow. *J. Fluid Mech.* **164**, 449–467.

SAFFMAN, P. G. 1965 The lift on a small sphere in a slow shear flow. *J. Fluid Mech.* **22**, 385–400 (and Corrigendum **31**, 1968, 624).

SCHLICHTING, H. 1987 *Boundary Layer Theory*, 7th edn. McGraw-Hill.

SPALART, P. R. 1988 Direct simulation of a turbulent boundary layer up to $Re = 1410$. *J. Fluid Mech.* **187**, 61–98.

TENNEKES, H. & LUMLEY, J. L. 1972 *A First Course in Turbulence*. MIT Press.